Rapid fault healing after seismic slip

John D. Bedford[1*], Takehiro Hirose[1] and Yohei Hamada[1]

[1]Kochi Institute for Core Sample Research (X-star), Japan Agency for Marine-Earth Science and Technology (JAMSTEC), 200 Monobe-otsu, Nankoku, Kochi 783-8502, Japan

*Corresponding author: John Bedford (j.bedford@jamstec.go.jp)

Abstract

Fault strength recovery (healing) following an earthquake is a key process in controlling the recurrence of future events; however, the rates and mechanisms of fault healing are poorly constrained. Here, by performing high-velocity friction experiments, we show that granite and gabbro fault gouges recover their strength rapidly after experiencing dynamic weakening during seismic slip. The healing rates are two orders of magnitude faster than those observed in typical frictional healing experiments performed at slow slip velocities. Analysis of the sheared gouges using Raman spectroscopy suggests that enhanced healing after seismic slip is associated with thermally activated chemical bonding at frictional contacts in the gouge. Our results imply that seismogenic faults regain their strength early during interseismic periods, indicating that healing may not be the dominant control on earthquake recurrence, with other processes, such as far-field tectonic loading or frictional stability transitions, likely dictating the occurrence of future events.

Teaser

Faults regain their strength rapidly after experiencing dynamic weakening during earthquake slip events.

1. Introduction

Faults slip suddenly during earthquakes, accelerating to velocities on the order of a few meters per second. At these seismic slip velocities a significant reduction in fault strength occurs(*1*) as a result of various dynamic weakening mechanisms becoming activated by shear heating(*2*). Although our knowledge of dynamic fault weakening processes has increased significantly over the last 25 years since the advent of high-velocity friction experiments(*3*), our understanding of how faults regain their strength after dynamic weakening, once seismic slip has ceased, is more limited. Fault restrengthening is a fundamental process in the earthquake cycle that may control the recurrence time(*4*), the maximum strength that can be attained(*5*, *6*), and the nature of radiated energy(*7*) in future events.

The rate of fault restrengthening can vary with both time and space along the fault during the earthquake cycle(*8*, *9*). Restrengthening may occur initially during coseismic slip itself, as sometimes observed during the deceleration phase of high-velocity friction experiments(*10*–*13*). Coseismic restrengthening (Fig. 1) is a potentially important process in the generation of pulse-like earthquake ruptures(*14*), which require that faults rapidly regain their strength (self-heal) after the passage of the rupture front. However, the mechanisms of coseismic restrengthening are poorly constrained and it is a phenomenon that is not always observed in experiments, or it may only partially recover the strength lost during high-velocity fault slip(*15*–*19*). In such cases, the majority of fault restrengthening must occur in the postseismic regime instead, when the fault is held in quasi-stationary contact.

The process of strength recovery as a fault is held in quasi-stationary contact, known as fault healing, has been extensively studied in experiments performed at slow sliding velocities (on the order of micrometers per second)(*20*). The common procedure for studying fault healing in the laboratory is to perform slide-hold-slide (SHS) experiments(*21*, *22*), whereby the shearing of fault materials is paused for predetermined durations and then shear strength is monitored as sliding is resumed after the hold period. Previous low-velocity SHS experiments have shown that frictional strength increases linearly with the logarithm of hold time, with healing rate being dependent on the composition of the fault materials(*23*).

The physical mechanisms responsible for fault healing are debated, with time-dependent growth of real contact area due to asperity creep often invoked to explain healing behavior(*24*). However, more recent work has suggested other processes such as chemical bond formation could be responsible for fault healing observed in laboratory experiments(*25*, *26*).

In some specific cases, the healing rates determined from low-velocity SHS experiments correlate well with stress drops observed during sequences of small repeating earthquakes in nature (i.e., the magnitude of the stress drop increases as the duration of the recurrence interval increases)(*4*, *27*). However, following large earthquakes, geophysical observations suggest rapid fault restrengthening can occur in comparison to typical recurrence intervals, with the majority of the strength being recovered early during the interseismic period. For example, shear-wave splitting measurements following the 1995 Kobe earthquake (moment magnitude M_w 6.9) on the Nojima fault indicate that the majority of fault strength had recovered within 33 months of the main event (recurrence interval of approximately 2000 years)(*28*). Borehole permeability measurements from the Longmenshan fault zone that hosted the 2008 Wenchuan earthquake (M_w 7.9), suggest that the fault healed within 0.6 to 2.5 years after the earthquake(*29*). Seismic velocity measurements made following the same event, and also the nearby 2013 Lushan earthquake (M_w 6.6), support the notion of rapid healing on the fault(*8*), with similar enhanced strength recovery rates also observed after the 2004 Parkfield earthquake (M_w 6.0) on the San Andreas fault(*9*). Geophysical observations thus potentially indicate that different postseismic healing processes are in operation immediately following large earthquakes, leading to more rapid restrengthening, than the classic "Dieterich-type" healing mechanisms(*21*, *24*) responsible for fault strengthening in low-velocity SHS experiments (Fig. 1). It should also be noted that over typical recurrence intervals of large earthquakes (up to several hundreds of years), processes such as pressure solution will increase cohesion of fault materials, contributing to the long-term strength evolution of the fault during interseismic periods(*30*–*32*).

In order to investigate rapid postseismic healing processes in the laboratory we need to simulate earthquake slip velocities, something that is not done in typical low-velocity SHS experiments. By shearing at seismic slip velocities, the fault materials will also experience dynamic weakening(*1*), which more closely mimics what happens during natural earthquakes. Here, we perform high-velocity (0.57 m/s) SHS experiments on gabbro and granite gouges under room humidity conditions at a constant normal stress of 1.5 MPa in all experiments (see Methods), to investigate how the gouges regain their strength during quasi-stationary hold periods after experiencing dynamic weakening. We varied the length of the static hold period in order to determine whether the postseismic restrengthening behavior exhibits either, (i) "Dieterich-type" healing as observed in low-velocity SHS experiments, (ii) a form of more rapid healing, or (iii) a combination of rapid and slow healing; as shown schematically in Figure 1. We then analyze the microstructures of the sheared gouges and perform Raman spectroscopy in an attempt elucidate the underlying healing mechanisms in operation after seismic slip events.

2. Results

Friction data

The frictional strength evolution of the granite and gabbro gouge samples is shown in Figure 2 for both sliding events in the SHS experiments. During the first high-velocity sliding event (slide 1) the gouge layers experience dynamic weakening with the friction coefficient (μ) decreasing by ~0.25, from a peak value between 0.7-0.8, to a final value of ~0.5 after 15 m of slip (Fig. 2a and c). During the static hold period between sliding events the gouge undergoes healing, with the peak friction of the second sliding event (slide 2) being dependent on the duration of the hold period (Fig. 2b and d) – i.e., longer hold periods lead to higher peak friction values. During slide 2, after reaching their respective peak friction values, the gouge layers again experience dynamic weakening, returning to a final μ of ~0.5 after another 15 m of high-velocity slip.

The gouge samples recover their strength rapidly during the static hold period, as shown in Figure 3 where $\Delta\mu$ (the difference between the peak friction of slide 2 (μ_{p2}) and the final friction of slide 1 (μ_{f1}),

$\Delta\mu = \mu_{p2} - \mu_{f1}$; see also Fig. S1) is plotted against hold time. After around 20 s of static hold, the granite gouge had recovered the majority of the strength it lost during slide 1, with the gabbro gouge healing even more rapidly (<10 s of static hold). For comparison, healing data from low-velocity SHS experiments performed on intact samples of granite and gabbro at slip rates of 2.6 μm/s has been included in Figure 3 (see Methods for more details). The healing rate ($\beta = \Delta\mu/\Delta\log{(t_h)}$, where t_h is the hold time) is around two orders of magnitude greater for the experiments performed at seismic slip velocities than those performed at micrometer per second slip velocities (Fig. 3). After the initial rapid strength recovery in the high-velocity tests, the healing rate decreased to a rate that is comparable to those observed in the low-velocity SHS experiments.

A major difference between high-velocity and low-velocity SHS experiments is that during high-velocity slip there is a large temperature increase caused by shear heating, which is much less significant during sliding at low-velocity. In order to measure the temperature evolution in our high-velocity SHS experiments, we placed thermocouples next to the upper surface of the gouge layer on the stationary side of the fault in some experiments (see Methods). We recorded peak temperatures of around 350-400 °C during the high-velocity sliding events, with the temperature decaying as the samples cooled during the hold period, returning to the ambient temperature in the laboratory after several minutes of static hold (Fig. 3). However, we find that the rapid frictional healing, which begins immediately after the initiation of the hold period, occurred when the gouge layer was still relatively hot, at temperatures >200 °C (Fig. 3).

Microstructural analysis and Raman spectroscopy

We analyzed the microstructures of the sheared gouges by collecting backscatter electron (BSE) and secondary electron (SE) images using a JEOL JSM-6500F field emission scanning electron microscope (FE-SEM). Fig. 4a-b shows BSE images of granite and gabbro gouge samples after the SHS experiments, where the sheared layers have been cut perpendicular to the shear plane and parallel to the shearing direction at a distance equal to 2/3 of the sample radius. (Note that the gouge layers were vacuum impregnated with a low-viscosity epoxy resin before being cut and polished ready for BSE imaging). The sheared gouges display a texture of well-rounded larger relict grains surrounded by fine-grained highly comminuted material, indicating that they have undergone a significant grain size reduction and particle roundening when compared to the starting gouge material (see Fig. S2), with this likely occurring via mechanical grinding(*33*). In the granite gouge the deformation appears to be homogeneously distributed across the layer (Fig. 4b), whereas the gabbro gouge displays evidence of a highly comminuted localized zone at the boundary of the layer (Fig. 4a and c). Despite the apparent difference in localization behavior between the different materials, their mechanical behavior is remarkably similar (Fig. 2), suggesting that shear localization does not have a strong control on frictional strength evolution under these experimental conditions. Our experiments were run under relatively low normal stress, previous studies suggest that localization would become more prominent if the gouge layers were sheared under higher normal stress(*34*, *35*), or if they were taken to greater shear strains(*36*).

The rapid healing observed after sliding at seismic slip rates in our experiments (Fig. 3) must be caused by a strengthening of the frictional contacts in the gouge layer, possibly as a result of enhanced interfacial chemical bonding. To investigate further the possible causes of the rapid restrengthening, we analyzed the sheared gouges using Raman spectroscopy (see Methods), as this provides information about the chemical structure of the gouge surface. We found that the gouges sheared at high-velocity all showed the appearance of a small broad peak in the Raman spectra at a wavenumber of ~1600 cm^{-1} (Fig. 4e and f), which corresponds to the bending vibrational mode of water(*37*) adsorbed on the surface of the gouge. This peak was not observed for the starting material or for samples sheared at low sliding velocities, only for samples that had been subjected to sliding at seismic slip rates.

We hypothesize that the switch in vibration mode of adsorbed water is caused by a change in chemical bonding on the gouge surface, potentially induced by elevated temperatures during high-velocity shearing, which could be responsible for the rapid healing observed in the SHS experiments (Fig. 3). To investigate this further, we heated undeformed samples of granite and gabbro in an oven to different temperatures (leaving them for ~20 minutes at the target temperature), the samples were then removed from the oven and left to cool at room atmosphere conditions (i.e., the same cooling conditions that the gouge layers experienced during the hold period of the SHS experiments). We analyzed the oven-heated samples using Raman spectroscopy and found the appearance of a small broad peak at ~1600 cm^{-1} for samples that had been heated to temperatures ≥250 °C (Fig. 4g and h), which is similar to the temperatures that the gouge layers experienced during high-velocity shearing where a similar Raman peak was observed (Fig. 4e and f) and also the temperature conditions where rapid healing occurred (Fig. 3). We note that the size of the adsorbed water peak in the oven-heated samples is often less than observed for the sheared gouge samples (particularly for granite), which may be a result the sheared gouges having a much greater surface area due to the presence of nanoparticles (Fig. 4d), producing a stronger Raman signal.

Discussion

The frictional strength data from our high-velocity SHS experiments show that the fault gouges heal rapidly during static hold periods after shearing at seismic slip rates, in comparison to typical healing rates observed in low-velocity SHS experiments performed at micrometer-per-second slip rates(*20*–*23*) (Fig. 3). The rapid healing rates we observe for the granite and gabbro gouges in our study are a similar order to those observed in previous high-velocity SHS experiments on clay-carbonate-bearing gouges from the Longmenshan fault system (sheared at 0.8 MPa normal stress and a slip rate of 1.4 m/s)(*19*), suggesting that rapid healing after high-velocity slip may be a universal phenomenon that is largely insensitive to the lithology of the fault materials. Elevated healing rates have also been observed in experiments performed at subseismic slip rates (on the order of a few millimeters-per-second)(*38*, *39*), however the healing rates in these experiments are an order of magnitude lower than we observe in our experiments at seismic slip velocities.

Dynamic weakening during the high-velocity shearing events in our experiments (Fig. 2) is likely caused by a combination of flash heating at asperity contacts(*40*) and the formation of amorphous wear materials in the gouge(*41*). X-ray diffraction analysis of the sheared gouges confirms the presence of amorphous material that was not present in the starting materials (Fig. S3). The microstructures of the sheared gouges (Fig. 4a-d) show no evidence of other weakening mechanisms that have been reported in previous studies such as frictional melting(*42*), silica-gel formation(*38*) or grain-size sensitive flow(*43*, *44*). Fault restrengthening during the hold periods is likely caused by the reformation of bonds at asperity contacts in the gouge material. There are two prevailing hypotheses for the time-dependent strengthening of frictional contacts during fault healing: (i) an increase in real contact area by asperity creep(*24*) (often referred to as the contact 'quantity' hypothesis), or (ii) the formation of chemical bonds across the asperity interface(*25*, *26*) (often referred to as the contact 'quality' hypothesis).

If we first consider asperity creep, it is plausible that this process would be more active after seismic slip, as creep is temperature-sensitive and the rapid healing we observe occurs immediately after high-velocity slip while the gouge is still relatively hot (>200 °C, Fig. 3). The likely mechanisms that could facilitate asperity creep are either solution-transfer processes(*45*) or indentation creep(*46*). Solution-transfer is unlikely to be a dominant mechanism in our experiments as they were run without a pore-fluid (i.e., room atmosphere conditions), therefore there is no solute to transfer chemical species. Furthermore, previous fault healing experiments under hydrothermal conditions, where solution-transfer processes are operative, show complex healing behavior(*31*, *47–49*) that is quite different to the healing trends we observe in our data (Fig. 3). Indentation creep can operate under atmospheric conditions in the absence of a pore-fluid(*50*), however, although previous low-velocity fault healing experiments at elevated temperatures (up to 550°C) under room humidity conditions indicate some temperature-dependence on healing rate(*51*, *52*), the effect is relatively minor and insufficient to explain the rapid healing in our experiments. It is therefore unlikely that an increase in the real contact area via asperity creep is the cause of the rapid restrengthening we observe during the static hold periods.

Alternatively, rapid healing may be caused by enhanced chemical bonding across contacting asperity interfaces. Our Raman data reveal a change in chemical bonding on the surface of the gouges sheared at high-velocity, with a switch in the vibrational mode of adsorbed water to the H-O-H bending mode, which only occurs after sample has been heated to temperatures ≥250 °C (Fig. 4g-h). Although we observe a change in adsorbed water properties, we do not expect the adsorbed water itself to be responsible for the rapid healing, as rapid healing occurs at temperatures >200 °C (Fig. 3) where water would be in the vapor state and desorbed from the gouge surface(*53*). Instead, we hypothesize that the rapid healing is a result of hydrogen bonding on the surface of the sheared gouge materials, which subsequently causes water to re-adsorb in the bending vibrational mode once the gouge has cooled to sufficiently low temperatures (<140 °C)(*53*) during the hold period. Hydrogen bonding can arise between hydroxylated silanol (Si-OH) surfaces(*54*), which are readily formed on freshly cleaved surfaces of silicate materials during frictional slip(*37*, *41*, *55*) (Fig. 5a). Once slip has stopped, the formation of hydrogen bonds between silanol surfaces can take place on very short timescales ($<10^{-2}$ s)(*56*). Therefore, if hydrogen bonding occurs during the first few seconds of static hold in our experiments, it could be responsible for the rapid increase in friction we observe. Furthermore, at elevated temperatures, like those produced by shear heating in our experiments, silanol groups on opposite sides of an asperity interface can react to form strong covalent siloxane (Si-O-Si) bonds(*57*, *58*) (Fig. 5b). Previous molecular dynamics simulations of silica-silica interfaces have shown that siloxane bond formation provides a plausible explanation for frictional healing, with frictional strength being approximately proportional to the number of siloxane bonds(*59*) and the kinetics of interfacial bond formation leading to a logarithmic time-dependent increase in strength(*56*), as observed in SHS experiments (Fig. 3). Therefore, we postulate that rapid healing after high-velocity slip is caused by either hydrogen or siloxane bond formation (or a combination of both) at asperity contacts in the sheared gouges. Once the gouge has cooled to sufficiently low temperature water will re-adsorb(*53*) (Fig. 5c). The vibrational motions of water molecules are sensitive to local hydrogen bonding on the adsorbent surface(*37*, *58*), thus the switch to the H-O-H bending mode we observe on the sheared gouges likely results from changes in the hydrogen bonding on the gouge surface that occur during/after high-velocity slip while the gouge is still hot, hence why the change in adsorbed water properties is only observed in samples that have been heated to temperatures >250 °C (Fig. 4g-h) and not in the samples sheared at low velocity where the temperature increase was low.

Regardless of the underlying restrengthening mechanism, our data clearly show that fault materials heal rapidly after seismic slip, which has important implications for our understanding of the earthquake cycle. Rapid healing may explain why geophysical observations suggest faults can regain their strength early during interseismic periods after large earthquakes(*28*, *29*). Fast-acting healing mechanisms, like those in operation during our experiments, potentially also operate during coseismic slip on natural faults, particularly when slip occurs heterogeneously along the fault such as during the propagation of pulse-like ruptures(*14*, *60*). The passage of a rupture pulse requires rapid healing in the just-slipped portions of the fault(*61*), in order for them to stay locked and prevent further slip as they are reloaded by waves from the actively slipping regions elsewhere along the fault. Results from recent dynamic rupture experiments further highlight the complex interplay between rapid weakening and healing processes that occur in gouge samples during dynamic rupture propagation(*62*).

Rapid fault strength recovery immediately following a seismic event suggests that earthquake recurrence is not necessarily controlled by continuous restrengthening over time during interseismic periods. Instead, if the majority of strength is recovered early during the interseismic period, as implied by our results, then earthquake recurrence on natural faults may be more strongly controlled by far-field tectonic loading (i.e., when the stress applied to the fault exceeds the strength an earthquake may occur). Alternatively, other time-dependent processes in operation during interseismic periods may influence earthquake recurrence. For example, over typical recurrence intervals of hundreds of years, fault cohesion will increase by processes such a pressure solution(*30*–*32*). Increased cohesion will not only contribute to the fault strength evolution, but will also influence the frictional stability of the gouge materials, with more cohesive materials often displaying rate-weakening behavior required for earthquake nucleation(*63*, *64*). It is plausible that transitions from rate-strengthening to rate-weakening behavior may occur as the gouge materials become more lithified during interseismic periods, potentially leading to earthquake recurrence once the frictional properties have evolved to state that promotes earthquake nucleation and unstable slip.

In summary, we find that faults regain their strength rapidly after experiencing dynamic weakening during seismic slip. After the initial rapid increase in strength, the healing rate decreases to a rate that is comparable to those observed in low-velocity friction experiments. Rapid healing occurs while the gouge is still hot from shear heating, and is likely promoted by enhanced chemical bonding across contacting asperity interfaces. Further experimental and theoretical studies are needed to investigate the kinetics of interfacial reactions over the range of stress, temperature and pore fluid conditions that faults experience during and after earthquake slip, to understand better strength recovery at seismogenic depths. Our findings motivate further study aimed at the quantification of rapid healing mechanisms and incorporation into larger-scale constitutive laws for modelling dynamic fault processes, to provide insight into the driving mechanisms of earthquake rupture and arrest, and hence seismic hazard.

Methods

Experimental procedure

The experimental samples were produced by crushing and sieving intact samples of Inada granite and Belfast gabbro to form simulated fault gouges (powders) with grain sizes between 63-125 μm. A layer of simulated gouge (measured by weight to produce a layer with an initial thickness of 1.5 mm) was then sandwiched between two cylindrical stainless steel experimental forcing blocks (diameter = 25 mm). The surface of the blocks contains radial grooves (0.5 mm deep) to minimize boundary shear between the gouge layer and the forcing blocks during the experiments. To limit gouge loss during shearing, the gouge layer was contained laterally by a 5 mm thick polytetrafluoroethylene (PTFE) sleeve (Fig. S4). The low-friction PTFE sleeve was cut and tightened onto the forcing blocks using a hose clip (Fig. S4), following the procedure outlined in the supplementary material of De Paola et al.,(*43*). We used a torque-screwdriver to ensure the hose clip was tightened by the same amount for each experiment. Once the gouge sample was constructed in between the forcing blocks, it was sheared using the PHV rotary shear apparatus(*65*) in the Rock Mechanics Laboratory at the Kochi Institute for Core Sample Research (Japan).

Before the main SHS experiment, the gouge samples were pre-sheared for four complete revolutions (equivalent to 0.2 m of slip) under a normal stress of 0.75 MPa at a rate of 1.7 mm/s, to ensure the gouge layer thickness was even across the sample. The normal stress was then increased to the experimental target value of 1.5 MPa. As all experiments were run under the same normal stress we did not correct for the shear stress contribution from the PTFE sleeve, with previous work showing that the mechanical contribution from the PTFE is negligible(*15*). All tests were conducted under room temperature (22-25 °C) and humidity (30-50%) conditions. During the main SHS experiments the gouge layers were sheared at 650 rpm for 285 revolutions (slide 1), they were then held in quasi-stationary contact for a predetermined amount of time, before being sheared again for another 285 revolutions at 650 rpm (slide 2). As the slip velocity varies with radial position, we use an "equivalent slip velocity" (v_e) which corresponds to the velocity at 2/3 of the radius of the cylindrical specimens(*43*), given by:

$$v_e = \frac{4\pi R r}{3}$$

where R is the revolution rate of the motor and r is the sample radius. In our experiments, a revolution rate of 650 rpm corresponds to an equivalent slip velocity of 0.57 m/s. During each sliding event the gouge layer was sheared for 285 revolutions which corresponds to an equivalent slip displacement (d_e) of ~15 m ($d_e = v_e t$ where t is time).

In some of the high-velocity experiments temperature measurements were made by placing thermocouples next to the upper surface of the gouge layer. Two holes were drilled into the upper experimental forcing block (on the stationary side of the fault) and thermocouples were inserted into the holes and sealed into place using a ceramic bond. The thermocouples were positioned at 2/3 of the radius so that the temperature measurements were consistent with the calculated v_e and d_e.

As well as the high-velocity SHS experiments, some additional tests were performed at micrometer-per-second slip velocities to compare healing rates after low-velocity slip with the rates determined in our high-velocity experiments (Fig. 3). In the low-velocity SHS experiments (performed at an equivalent slip velocity of 2.6 $\mu m \cdot s^{-1}$) we used intact cylindrical rock-to-rock samples of Inada granite and Belfast gabbro, instead of gouge. Initially we tried performing the low-velocity SHS experiments using gouge samples, however, we found negligible healing even after hold periods >1000 s (healing rate, $\beta \approx 0$). As the purpose of our low-velocity SHS experiments is just to provide an approximate representation of typical healing rates at slow sliding velocities, we chose to instead include data from rock-to-rock samples in Fig. 3, as the healing rates we determined from the rock-to-rock samples are close to typical healing rates observed in many low-velocity healing studies(*22*, *23*). Prior to the low-velocity SHS experiments, the cylindrical rock samples were rotated for more than 1000 rotations at a constant speed of 4 rpm ($v_e = 3.5$ $mm \cdot s^{-1}$) over a range of incrementally increasing normal stresses from 0.3 to 1.4 MPa. The purpose of this procedure was to remove any heterogeneities and ensure the surfaces on opposites side of the sliding interface were parallel. The wear materials produced on the sliding surface during this pre-sliding were not removed before the SHS experiments, thus the rock samples were separated by a thin gouge layer during the experiments. The wear materials produced during the experiments were allowed to extrude from the slip zone (we did not use a PTFE containing ring for these tests). Once the sliding surface was prepared, the normal stress was increased to 1.5 MPa and the samples were sheared for 0.26 mm during each sliding event in the SHS experiment at a velocity of 2.6 $\mu m \cdot s^{-1}$; the length of the hold time between the sliding events was varied to determine the healing rate.

Raman spectroscopy

After the experiments the PTFE ring was removed and the sample holders were gently opened to expose the sheared gouge sample. The surface of the gouge was then analyzed using Raman spectroscopy. (Note that Raman spectra were acquired on the exposed gouge surface before it was impregnated with epoxy resin and prepared for microstructural imaging). Raman spectra of the test samples were obtained with a 514.5 nm Ar laser (Showa Optronics Co., Ltd.) and T64000 Raman system (Jobin Yvon Horiba). The laser passed through a 40× objective and the laser power at the sample surface was set at 2–5 mW. The scattered light was collected by backscattered geometry with a 25 μm pinhole and a holographic notch filter, and finally dispersed using a 1800 grids/mm grating and analyzed by a Peltier cooled CCD detector (SPECTRUM ONE, Jobin Yvon Horiba). Spatial resolution is about 1 μm, and wavenumber resolution is about 1 cm^{-1}. Frequencies of the Raman bands were calibrated by measuring silicon standards.

References

1. G. Di Toro, R. Han, T. Hirose, N. De Paola, S. Nielsen, K. Mizoguchi, F. Ferri, M. Cocco, T. Shimamoto, Fault lubrication during earthquakes. *Nature*. **471**, 494–498 (2011).

2. T. E. Tullis, "Mechanisms for friction of rock at earthquake slip rates" in *Treatise on Geophysics*, G. Schubert, Ed. (Elsevier, ed. 2nd, 2015), vol. 4, pp. 139–159.

3. A. Tsutsumi, T. Shimamoto, High-velocity frictional properties of gabbro. *Geophys. Res. Lett.* **24**, 699–702 (1997).

4. J. E. Vidale, W. L. Ellsworth, A. Cole, C. Marone, Variations in rupture process with recurrence interval in a repeated small earthquake. *Nature*. **368**, 624–626 (1994).

5. H. Kanamori, C. R. Allen, "Earthquake repeat time and average stress drop" in *Earthquake Source Mechanics*, S. Das, J. Boatwright, C. H. Scholz, Eds. (American Geophysical Union, Washington D.C., 1986), vol. 37, pp. 227–235.

6. C. H. Scholz, C. A. Aviles, S. G. Wesnousky, Scaling differences between large interplate and intraplate earthquakes. *Bull. Seismol. Soc. Am.* **76**, 65–70 (1986).

7. G. C. McLaskey, A. M. Thomas, S. D. Glaser, R. M. Nadeau, Fault healing promotes high-

frequency earthquakes in laboratory experiments and on natural faults. *Nature*. **491**, 101–104 (2012).

8. S. Pei, F. Niu, Y. Ben-Zion, Q. Sun, Y. Liu, X. Xue, J. Su, Z. Shao, Seismic velocity reduction and accelerated recovery due to earthquakes on the Longmenshan fault. *Nat. Geosci.* **12**, 387–392 (2019).

9. Y.-G. Li, P. Chen, E. S. Cochran, J. E. Vidale, T. Burdette, Seismic evidence for rock damage and healing on the San Andreas Fault associated with the 2004 M 6.0 Parkfield earthquake. *Bull. Seismol. Soc. Am.* **96**, S349–S363 (2006).

10. H. Sone, T. Shimamoto, Frictional resistance of faults during accelerating and decelerating earthquake slip. *Nat. Geosci.* **2**, 705–708 (2009).

11. C. Harbord, N. Brantut, E. Spagnuolo, G. Di Toro, Fault friction during simulated seismic slip pulses. *J. Geophys. Res. Solid Earth.* **126**, e2021JB022149 (2021).

12. M. Violay, F. Passelegue, E. Spagnuolo, G. Di Toro, C. Cornelio, Effect of water and rock composition on re-strengthening of cohesive faults during the deceleration phase of seismic slip pulses. *Earth Planet. Sci. Lett.* **522**, 55–64 (2019).

13. B. P. Proctor, T. M. Mitchell, G. Hirth, D. Goldsby, F. Zorzi, J. D. Platt, G. Di Toro, Dynamic weakening of serpentinite gouges and bare surfaces at seismic slip rates. *J. Geophys. Res. Solid Earth*. **119**, 8107–8131 (2014).

14. T. H. Heaton, Evidence for and implications of self-healing pulses of slip in earthquake rupture. *Phys. Earth Planet. Inter.* **64**, 1–20 (1990).

15. C. E. Seyler, J. D. Kirkpatrick, H. M. Savage, T. Hirose, D. R. Faulkner, Rupture to the trench? Frictional properties and fracture energy of incoming sediments at the Cascadia subduction zone. *Earth Planet. Sci. Lett.* **546**, 116413 (2020).

16. L. B. Hunfeld, J. Chen, A. R. Niemeijer, S. Ma, C. J. Spiers, Seismic slip-pulse experiments simulate induced earthquake rupture in the Groningen gas field. *Geophys. Res. Lett.* **48**, e2021GL092417 (2021).

17. C. Boulton, L. Yao, D. R. Faulkner, J. Townend, V. G. Toy, R. Sutherland, S. Ma, T. Shimamoto, High-velocity frictional properties of Alpine Fault rocks: Mechanical data, microstructural analysis, and implications for rupture propagation. *J. Struct. Geol.* **97**, 71–92 (2017).

18. R. Han, T. Shimamoto, T. Hirose, J. H. Ree, J. Ando, Ultralow friction of carbonate faults caused by thermal decomposition. *Science*. **316**, 878–881 (2007).

19. L. Yao, T. Shimamoto, S. Ma, R. Han, K. Mizoguchi, Rapid postseismic strength recovery of Pingxi fault gouge from the Longmenshan fault system: Experiments and implications for the mechanisms of high-velocity weakening of faults. *J. Geophys. Res. Solid Earth*. **118**, 4547–4563 (2013).

20. C. Marone, D. M. Saffer, "The mechanics of frictional healing and slip instability during the seismic cycle" in *Treatise on Geophysics*, G. Schubert, Ed. (Elsevier, ed. 2nd, 2015), vol. 4, pp. 111–138.

21. J. H. Dieterich, Time-dependent friction in rocks. *J. Geophys. Res.* **77**, 3690–3697 (1972).

22. C. Marone, On the rate of frictional healing and the constitutive law for time- and slip-dependent friction. *Int. J. Rock Mech. Min. Sci.* **34**, (1997).

23. B. M. Carpenter, M. J. Ikari, C. Marone, Laboratory observations of time-dependent frictional strengthening and stress relaxation in natural and synthetic fault gouges. *J. Geophys. Res. Solid Earth*. **121**, 1183–1201 (2016).

24. J. H. Dieterich, B. D. Kilgore, Direct observation of frictional contacts: New insights for state-dependent properties. *Pure Appl. Geophys.* **143**, 283–302 (1994).

25. Q. Li, T. E. Tullis, D. Goldsby, R. W. Carpick, Frictional ageing from interfacial bonding and the origins of rate and state friction. *Nature*. **480**, 233–236 (2011).

26. C. A. Thom, R. W. Carpick, D. L. Goldsby, Constraints on the physical mechanism of frictional aging from nanoindentation. *Geophys. Res. Lett.* **45**, 13306–13311 (2018).

27. C. Marone, J. E. Vidale, W. L. Ellsworth, Fault healing inferred from time dependent variations in source properties of repeating earthquakes. *Geophys. Res. Lett.* **22**, 3095–3098 (1995).

28. K. Tadokoro, M. Ando, Evidence for rapid fault healing derived from temporal changes in S wave splitting. *Geophys. Res. Lett.* **29**, 1047 (2002).

29. L. Xue, H.-B. Li, E. E. Brodsky, Z.-Q. Xu, Y. Kano, H. Wang, J. J. Mori, J.-L. Si, J.-L. Pei, W. Zhang, G. Yang, Z.-M. Sun, Y. Huang, Continuous permeability measurements record healing inside the Wenchuan earthquake fault zone. *Science*. **340**, 1555–1559 (2013).

30. E. Tenthorey, S. F. Cox, Cohesive strengthening of fault zones during the interseismic period: An experimental study. *J. Geophys. Res.* **111**, B09202 (2006).

31. M. P. A. van den Ende, A. R. Niemeijer, An investigation into the role of time-dependent cohesion in interseismic fault restrengthening. *Sci. Rep.* **9**, 9894 (2019).

32. S. K. Muhuri, T. A. Dewers, T. E. Scott Jr., Z. Reches, Interseismic fault strengthening and earthquake-slip instability: Friction or cohesion? *Geology*. **31**, 881–884 (2003).

33. C. G. Sammis, Y. Ben-Zion, Mechanics of grain-size reduction in fault zones. *J. Geophys. Res. Solid Earth*. **113**, B02306 (2008).

34. M. Rempe, G. Di Toro, T. M. Mitchell, S. A. F. Smith, T. Hirose, J. Renner, Influence of effective stress and pore fluid pressure on fault strength and slip localization in carbonate slip zones. *J. Geophys. Res. Solid Earth*. **125**, e2020JB019805 (2020).

35. J. D. Bedford, D. R. Faulkner, The role of grain size and effective normal stress on localization

and the frictional stability of simulated quartz gouge. *Geophys. Res. Lett.* **48**, e2020GL092023 (2021).

36. S. Kaneki, K. Oohashi, T. Hirono, H. Noda, Mechanical amorphization of synthetic fault gouges during rotary-shear friction experiments at subseismic to seismic slip velocities. *J. Geophys. Res. Solid Earth*. 125, e2020JB019956 (2020).

37. A. K. Kronenberg, "Hydrogen speciation and chemical weakening of quartz" in *Silica: Physical Behaviour, Geochemistry and Materials Applications*, P. J. Heaney, C. T. Prewitt, G. V Gibbs, Eds. (Mineralogical Society of America, 1994), pp. 123–176.

38. D. L. Goldsby, T. E. Tullis, Low frictional strength of quartz rocks at subseismic slip rates. *Geophys. Res. Lett.* **29**, 1844 (2002).

39. G. Di Toro, D. L. Goldsby, T. E. Tullis, Friction falls towards zero in quartz rock as slip velocity approaches seismic rates. *Nature*. **427**, 436–439 (2004).

40. J. R. Rice, Heating and weakening of faults during earthquake slip. *J. Geophys. Res.* **111**, B05311 (2006).

41. C. D. Rowe, K. Lamothe, M. Rempe, M. Andrews, T. M. Mitchell, G. Di Toro, J. C. White, S. Aretusini, Earthquake lubrication and healing explained by amorphous nanosilica. *Nat. Commun.* **10**, 1–11 (2019).

42. T. Hirose, T. Shimamoto, Growth of molten zone as a mechanism of slip weakening of simulated faults in gabbro during frictional melting. *J. Geophys. Res.* **110**, B05202 (2005).

43. N. De Paola, R. E. Holdsworth, C. Viti, C. Collettini, R. Bullock, Can grain size sensitive flow lubricate faults during the initial stages of earthquake propagation? *Earth Planet. Sci. Lett.* **431**, 48–58 (2015).

44. G. Pozzi, N. De Paola, S. B. Nielsen, R. E. Holdsworth, T. Tesei, M. Thieme, S. Demouchy,

Coseismic fault lubrication by viscous deformation. *Nat. Geosci.* **14**, 437–442 (2021).

45. E. H. Rutter, Pressure solution in nature, theory and experiment. *J. Geol. Soc. London.* **140**, 725–740 (1983).

46. C. H. Scholz, J. T. Engelder, The role of asperity indentation and ploughing in rock friction - I. Asperity creep and stick-slip. *Int. J. Rock Mech. Min. Sci. Geomech. Abstr.* **13**, 149–154 (1976).

47. S. L. Karner, C. Marone, B. Evans, Laboratory study of fault healing and lithification in simulated fault gouge under hydrothermal conditions. *Tectonophysics*. **277**, 41–55 (1997).

48. T. Jeppson, D. Lockner, "Impact of fluid-rock interaction on strength and hydraulic transmissivity evolution in shear fractures under hydrothermal conditions" in *47th Workshop on Geothermal Reservoir Engineering* (Stanford, California, 2022).

49. M. Nakatani, C. H. Scholz, Frictional healing of quartz gouge under hydrothermal conditions: 1. Experimental evidence for solution transfer healing mechanism. *J. Geophys. Res.* **109**, B07201 (2004).

50. K. M. Frye, C. Marone, Effect of humidity on granular friction at room temperature. *J. Geophys. Res.* **107**, 2309 (2002).

51. E. K. Mitchell, Y. Fialko, K. M. Brown, Temperature dependence of frictional healing of Westerly granite: Experimental observations and numerical simulations. *Geochemistry, Geophys. Geosystems*. **14**, 567–582 (2013).

52. M. Nakatani, Conceptual and physical clarification of rate and state friction: Frictional sliding as a thermally activated rheology. *J. Geophys. Res.* **106**, 13347–13380 (2001).

53. Z. Reches, D. A. Lockner, Fault weakening and earthquake instability by powder lubrication. *Nature*. **467**, 452–455 (2010).

54. T. A. Michalske, E. R. Fuller, Closure and repropagation of healed cracks in silicate glass. *J. Am.

Ceram. Soc. **68**, 586–590 (1985).

55. T. Hirose, S. Kawagucci, K. Suzuki, Mechanoradical H2 generation during simulated faulting: Implications for an earthquake-driven subsurface biosphere. *Geophys. Res. Lett.* **38**, L17303 (2011).

56. Y. Liu, I. Szlufarska, Chemical origins of frictional aging. *Phys. Rev. Lett.* **109**, 186102 (2012).

57. G. Vigil, Z. Xu, S. Steinberg, J. Israelachvili, Interactions of silica surfaces. *J. Colloid Interface Sci.* **165**, 367–385 (1994).

58. S. Shioji, M. Kawaguchi, Y. Hayashi, K. Tokami, H. Yamamoto, Rehydroxylation of dehydrated silica surfaces by water vapor adsorption. *Adv. Powder Technol.* **12**, 331–342 (2001).

59. A. Li, Y. Liu, I. Szlufarska, Effects of interfacial bonding on friction and wear at silica/silica interfaces. *Tribol. Lett.* **56**, 481–490 (2014).

60. V. Lambert, N. Lapusta, S. Perry, Propagation of large earthquakes as self-healing pulses or mild cracks. *Nature*. **591**, 252–258 (2021).

61. G. Perrin, J. R. Rice, G. Zheng, Self-healing slip pulse on a frictional surface. *J. Mech. Phys. Solids*. **43**, 1461–1495 (1995).

62. V. Rubino, N. Lapusta, A. J. Rosakis, Intermittent lab earthquakes in dynamically weakening fault gouge. *Nature*. **606**, 922–929 (2022).

63. M. J. Ikari, A. Hüpers, Velocity-weakening friction induced by laboratory-controlled lithification. *Earth Planet. Sci. Lett.* **554**, 116682 (2021).

64. A. Roesner, M. J. Ikari, D. M. Saffer, K. Stanislowski, A. M. Eijsink, A. J. Kopf, Friction experiments under in-situ stress reveal unexpected velocity-weakening in Nankai accretionary prism samples. *Earth Planet. Sci. Lett.* **538** (2020), doi:10.1016/j.epsl.2020.116180.

65. W. Tanikawa, H. Mukoyoshi, O. Tadai, Experimental investigation of the influence of slip

velocity and temperature on permeability during and after high-velocity fault slip. *J. Struct. Geol.* **38**, 90–101 (2012).

Acknowledgments

We are grateful to T. Suzuki and O. Tadai for technical support with the experiments and analyses.

Funding

This work was supported by a Japan Society for the Promotion of Science (JSPS) International Research Fellowship and JSPS KAKENHI Grant Numbers JP20F20786 and JP19K21907.

Author Contributions

Conceptualization: JDB, TH, YH

Methodology: JDB, TH, YH

Investigation: JDB, YH

Visualization: JDB

Writing – original draft: JDB

Writing - review and editing: JDB, TH, YH

Competing Interests

The authors declare they have no competing interests.

Data and Materials Availability

The associated experimental data files for this research can be accessed at:

https://data.mendeley.com/datasets/rw3ndtwkgt/1

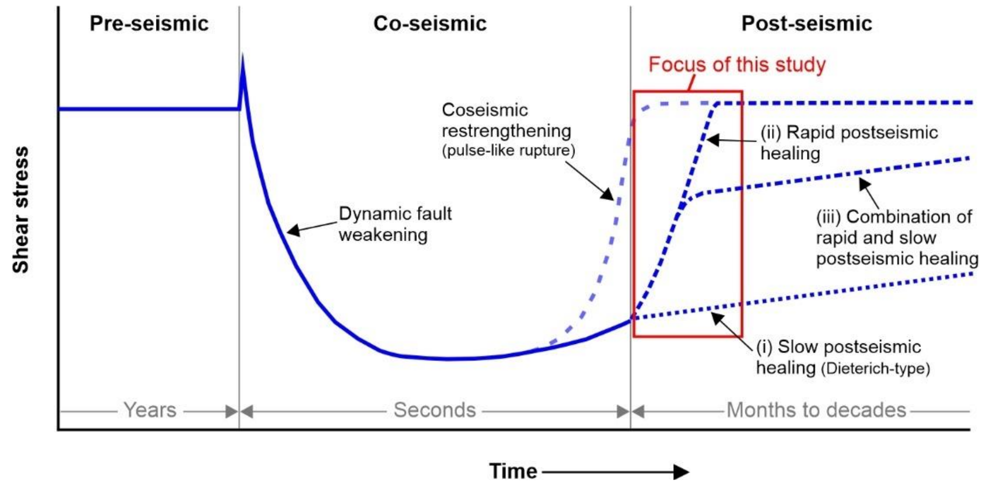

Fig. 1. Schematic diagram of fault strength evolution during the seismic cycle. During coseismic slip, a significant reduction in shear stress occurs as a result of dynamic fault weakening. In the postseismic regime the fault regains its strength as it is held in quasi-stationary contact. The aim of this study is to determine whether fault strength recovery immediately following seismic slip occurs via (i) slow "Dieterich-type" healing, (ii) rapid postseismic healing, or (iii) a combination of rapid and slow healing.

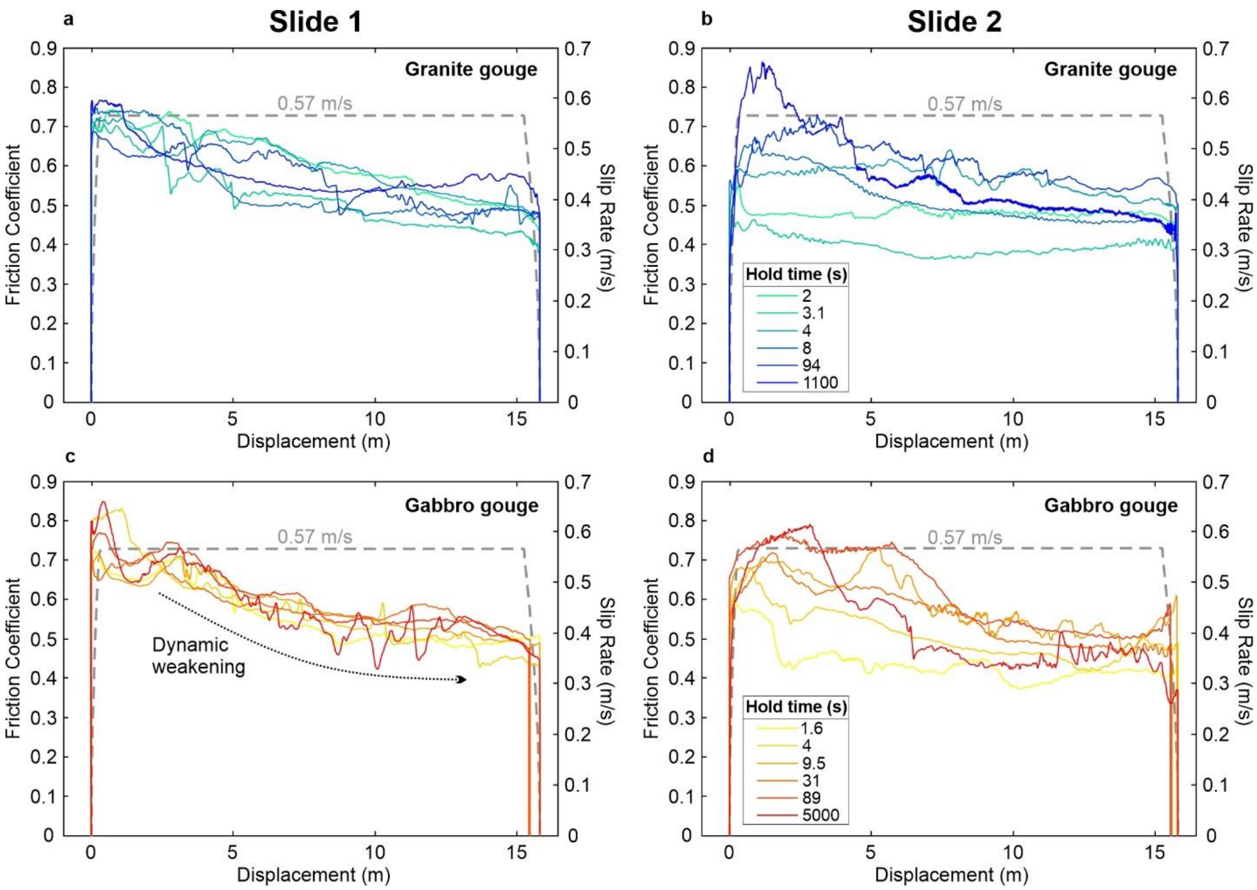

Fig. 2. Example mechanical data from the two high-velocity sliding events in the slide-hold-slide experiments. The plots show the evolution of the friction coefficient with displacement for the granite gouge during (**a**) the first sliding event (slide 1), and (**b**) the second sliding event (slide 2). The same data are shown for the gabbro gouge in panels (**c**) and (**d**), respectively. The velocity-displacement history during the experiments is shown by the grey dashed line. The gouge layers all show similar dynamic weakening during slide 1, with the friction coefficient decreasing by ~0.25 after 15 m of displacement. The peak friction during slide 2 is controlled by the duration of the static hold time between the sliding events, with longer hold times leading to higher peak friction.

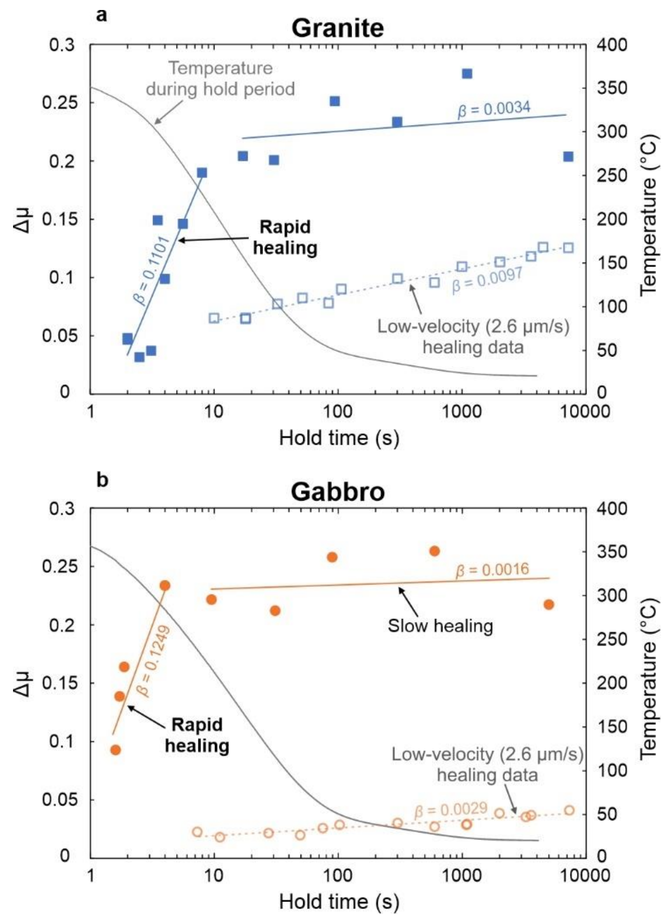

Fig. 3. Frictional healing data from the high-velocity SHS experiments. The slide-hold-slide parameter $\Delta\mu$ is plotted against hold time for (**a**) granite gouge and (**b**) gabbro gouge. The gouges experience rapid healing immediately after the initiation of the hold period; the healing rate then decreases to a rate comparable to those observed in low-velocity SHS experiments. Healing data from experiments performed at 2.6 μm/s has been included (hollow symbols) for comparison. The temperature evolution was monitored during the hold period (grey line); rapid healing occurs while the gouges are still relatively hot (>200 °C) after the high-velocity first sliding event.

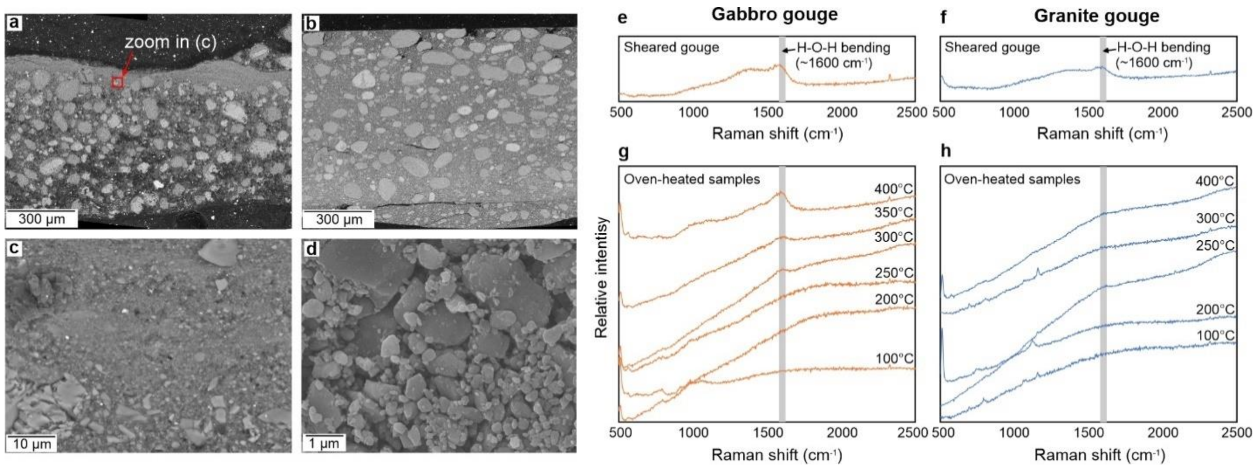

Fig. 4. Microstructures of the sheared gouges and Raman spectra. Backscatter electron images of (**a**) gabbro and (**b**) granite gouge layers recovered at the end of the SHS experiments. (**c**) Zoom of the localized zone within the gabbro gouge layer (from the red box in (a)). (**d**) Secondary electron image of the surface of the gabbro gouge layer showing the presence of sub-micron particles. (**e**) and (**f**) Raman spectra of the surface of the sheared gabbro and granite layers, respectively. Both show a broad peak at a wavenumber of ~1600 cm^{-1}, indicating the bending vibrational mode of H-O-H. Panels (**g**) and (**h**) show Raman spectra for undeformed gabbro and granite samples heated to different temperatures in an oven and then left to cool under atmospheric humidity conditions. The broad peak at 1600 cm^{-1} appears in samples that have been heated to temperatures ≥250 °C.

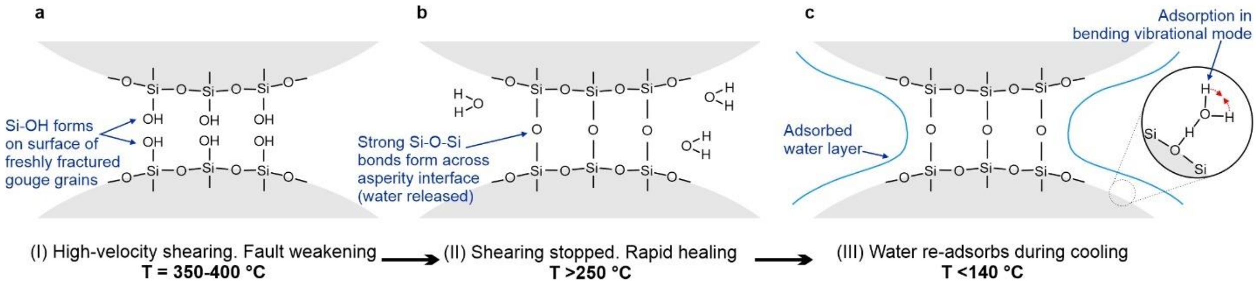

Fig. 5. Schematic cartoon showing the evolution of chemical bonding during and after high-velocity slip. (**a**) Silanol bonds (Si-OH) form on freshly fractured gouge surfaces during high-velocity slip. During the hold period, once fault slip has ceased, we hypothesize that rapid healing occurs as a result of either hydrogen bonding between adjacent silanol surfaces, or (**b**) the formation of strong siloxane bonds across the asperity interface. (**c**) Once the gouge has cooled to temperatures <140 °C during the hold period, water re-adsorbs onto the surface in the bending vibrational mode.